

# Investigation of Seismic Waveform and Co-seismic Displacements Based on GNSS Observations at CORS-TR Stations of Sofalaca-Şehitkamil Gaziantep (Mw:7.7) Earthquake on February 6, 2023 by Kinematic-Precise Point Positioning Technique



Baris Karadeniz\*

Department of Geomatics Engineering, Gebze Technical University, Türkiye

Submission: April 24, 2023; Published: May 19, 2023

\*Corresponding author: Baris Karadeniz, Department of Geomatics Engineering, Gebze Technical University, Gebze, Kocaeli, Türkiye

## Abstract

The high pressure created by the stretching or compression of the rocks on the earth causes the earth's crust to break and faults occur. These faults are found in many parts of the world and are actively seen in Türkiye. In this study, space and satellite techniques and geodetic results of the Sofalaca-Şehitkamil Gaziantep earthquake that occurred on the Eastern Anatolian Fault Zone on 06.02.2023 in Türkiye were evaluated. Stations recording GNSS observations at 1Hz sampling interval of the network of Continuously Operating Reference Stations, Türkiye (CORS-TR) were used, homogeneously distributed in and around the epicenter where the earthquake occurred. In order to examine the characteristics of the surface movements occurring at the time of the earthquake, the Kinematic-PPP technique and the 1 second RINEX data in the RTKLIB software were evaluated with both real-time and post-process solution approaches. With both solution approaches, displacement amounts and velocities, of the surface waveforms occurring at the time of the earthquake were calculated at all stations. In addition, the co-seismic displacements of the selected 23 stations after the earthquake were calculated and the changes on the surface of the earthquake were interpreted. At GNSS Stations, the maximum velocities during the earthquake were calculated in the range of 1.6-23.3cm/s for the north component, 0.5-13.5cm/s for the east component, and 1.9-24.6cm/s for the up component. The post-earthquake co-seismic displacements at stations were determined as 0.1-37.1 cm for the north component, 0.1-22.7cm for the east component and 0.1-20.0cm for the up component.

**Keywords:** Co-seismic displacement; Surface waveforms; CORS-TR; Kinematic-PPP

## Introduction

The shapes formed by the waters and land covering the earth are formed in different geological times from the past to the present. It is a rich country in terms of geology and geomorphology, as there is land belonging to all geological time periods in the formation of Türkiye. Although there are lands that were formed in the 1st and 2nd geological times in the country, their current appearance was formed in the last geological time period. In this context, Türkiye shows a young formation characteristic in tectonic sense. Therefore, there are many active faults in and around Türkiye. In this case, this region has become one of the active working areas of the world for the studies of scientists who carry out tectonic and seismic researches in the field of earthquakes. Türkiye is surrounded by the Eurasian Plate in the north, the African Plate in the south and the Arabian Plate in the southeast, and has the Anatolian Plate in its center [1-3].

The Anatolian Plate is moving westward about 21mm/year due to the surrounding tectonic plates [4,5]. In the north of the country, there is the North Anatolian Fault Zone (NAFZ), one of the most active faults in the world, with a right-lateral strike-slip fault type that forms the border of the Eurasian and Anatolian Plates [6,7]. On the other hand, there is the East Anatolian Phase Zone (EAFZ), which is the encounter area between the Arabian and Anatolian Plates and has left-lateral strike-slip fault type [2,8,9]. The EAFZ is one of the most important neotectonic faults, approximately 600km long, consisting of more than one fault segment, starting from Karlıova in the northeast of Türkiye and in the southwest direction between the Gulf of Iskenderun [10,11]. Some segments on this fault zone are shown as active faults [11,12]. Geodetic studies are suggested to examine the dynamic behavior of active faults on the fault zone [13].

In Nowadays, GNSS technology and different positioning algorithms are used in order to monitor the surface waveforms before, during and after the earthquake and to determine the co-seismic displacements [14-20]. High-precision 3D position information from GNSS data plays an important role in detecting dynamic behavior on the fault [21]. In addition to GNSS seismology, many scientific studies have been carried out by integrating GNSS sensors in areas such as structural health monitoring for the detection of damage to buildings during earthquakes, early warning systems for the pre-detection of natural disasters such as earthquakes or tsunamis [22-30]. As a result of the northward movement of the Arabian Plate in the southeast of the East Anatolian Fault and the westward movement of the Anatolian Plate in the northwest, the studies carried out on this fault at different times are approximately  $9\pm 1\text{mm/year}$  [31],  $5\text{-}8\text{mm/year}$  [32,33],  $10\text{mm/year}$  [4,34],  $13\text{mm/year}$  [35],  $11\pm 3\text{mm/year}$  and  $8\text{mm/year}$  [36], slip rates were calculated. Considering the earthquakes that occurred in paleo-seismology and instrumental periods in the segments on the EAFZ, it was revealed that there are seismic gaps in the Gölbaşı-Türkoğlu and Bingöl-Palu segments [32,37]. However, in the geodetic study conducted in this region, using GNSS data sets, the slip rate on the EAFZ was approximately  $10\text{ mm/year}$  in the north of the Gölbaşı-Türkoğlu segment, while it decreased to approximately  $4.5\text{mm/year}$  in the South [13]. In addition, the seismic gaps specified on the EAFZ in previous studies were expressed as Palu-Sincik and Çelikhan-Türkoğlu segments in this study, and it was concluded that earthquakes with a magnitude of  $M_w:7.4$  and  $M_w:7.7$  could occur, respectively [13]. With this study carried out in the region, it is revealed that a seismic activity may occur and the potential for loss of life and property is high. A proof of this is the  $M_w:6.8$  magnitude Sivrice (Elazığ) earthquake that occurred on January 24, 2020. With this earthquake, attention was drawn to the potential of active seismic movements in the region [38].

In this study, real-time detection of the seismic waveform and co-seismic displacements of the  $M_w: 7.7$  magnitude Sofalaca-Şehitkamil Gaziantep earthquake, which occurred on February 6, 2023, was made with the GNSS observation data recorded at the base GNSS stations connected to in the network of CORS-TR close to the region. The real-time Precise Point Positioning (RT-PPP) solution approach of displacements and velocities at the time of the earthquake was evaluated with reference to the PP-PPP approach. Displacements and velocities were calculated with an accuracy of about 1 cm vertically, at millimeter level horizontally, and the results were consistent with each other. In addition, the characteristics of the surface movements of the region were interpreted by calculating the post-earthquake co-seismic displacements.

### Materials and Method

#### 6 February 2023 sofalaca-şehitkamil gaziantep ( $M_w:7.7$ ) earthquake

On February 6, 2023, on the Eastern Anatolian Fault Zone, at

04:17, Türkiye Time (TRT), a very large earthquake with epicenter centered in Sofalaca-Şehitkamil-Gaziantep and instrumentally calculated by Kandilli Observatory and Earthquake Research Institute (KRDAE) as moment magnitude  $M_w:7.7$  and local magnitude  $ML:7.4$  occurred. The magnitude and location of the earthquake are shown in Figure 1 by different centers. According to the epicenter where the earthquake occurred, it is understood that it occurred within the borders of Gaziantep province. Although the depth of focus of the earthquake varies between 5 and 10 km for different centers, it is seen that it is a shallow earthquake [39]. Due to the shallowness and severity of the earthquake, it was felt strongly in Kahramanmaraş, Gaziantep, Diyarbakır, Şanlıurfa, Kilis, Adana, Malatya, Osmaniye, Adıyaman, Hatay and surrounding provinces within the borders of Eastern Anatolia, Southeastern Anatolia, Central Anatolia and Mediterranean Regions. According to the preliminary reports in the post-earthquake region, when the deformations caused by the earthquake on the land surface are examined, the fault type in many regions is expressed as left-lateral strike-slip. According to the results of the field studies between February 10 and February 16 by AFAD Earthquake Department, it was stated that the earthquake was effective in an area of approximately 108 thousand 812 square kilometers, together with 11 provinces and the surrounding provinces. In addition, in two consecutive earthquakes, the Sofalaca-Şehitkamil Gaziantep earthquake records were more effective in Hatay and Kahramanmaraş, considering the field studies and the evaluations of the people of the region. Although a 290km long fracture occurred in the region in terms of surface faulting, displacements of up to 6.5 meters were observed [40].

In urban areas, as a result of the loss of shear strength and hardness of the ground due to sudden displacements in case of shaking or stress during an earthquake, liquefaction in the ground and settlements and side-lyings have occurred in the buildings. In addition, the deformations caused by the surface faulting that continues under the structures have also caused the collapse or damage of the structures [40]. As of 20 March 2023, it was determined that 255 thousand buildings were destroyed or damaged in the region, it was stated that more than 50 thousand lives were lost and more than 107 thousand citizens were injured. Thus, the date of 06 February 2023, when two consecutive earthquakes occurred, was recorded as the most destructive earthquake in the history of Türkiye.

#### GNSS observations and evaluation

GNSS stations belonging to the network of CORS-TR were selected for real-time monitoring of the seismic surface waveform that occurred in the Sofalaca-Şehitkamil Gaziantep ( $M_w:7.7$ ) earthquake, and to determine the co-seismic displacements and velocities by examining the earth crust movements. These stations are located close to the epicenter of the earthquake and homogeneously distributed on the fault surface, approximately 30km to 375km from the earthquake epicenter, in Figure 2, point locations are shown. In order to see which type of faulting, in which direction the tectonic plates move, and the 3-dimensional

vector distribution of the distance from the center, 34 stations were selected in the selection of the stations to surround the fault surface. Observation data sets of selected stations in RINEX (Receiver Independent Exchange) format, dated 06.02.2023 with 1s interval, were obtained from the website of the CORS-TR System jointly operated by the General Directorate of Land Registry and Cadastre and the General Directorate of Mapping. Considering the GNSS data sets of the stations, GNSS observation data of the day of the earthquake did not record at ADY1, HAT2, MAR1, ONIY and MARD stations. In addition, after the evaluation of GNSS measurements, GNSS observations of SURF, KLS1, EKZ1, CYL2 and VIR2 station points were formed data interruption at 04.17 TRT (UTC 01.17) when the earthquake occurred. GNSS observation data of KAP1 station is also not available. For these reasons, the GNSS dataset of 11 stations was not evaluated. In the observations of GNSS stations with a sampling interval of 1 second, Galileo and BeiDou satellite observations were recorded as well as GPS and GLONASS satellite observations due to the characteristics of some receiver/antenna. However, in this study, solutions are based on GPS and GLONASS satellite observations to ensure integrity. Since GNSS datasets are in 1-hour sessions for each station, they are combined for 24 hours. GNSS observations of each station were evaluated with the kinematic-PPP technique in the rtkpost module of the open source code RTKLIB software. The surface waveforms of the 3-dimensional position component of each station were examined as 300 epochs (5 minutes) before the earthquake,

during and 300 epochs (5 minutes) after the earthquake. In addition, co-seismic displacements, velocities and statistical evaluations of the stations as a result of the 3-dimensional surface movements that occurred during the earthquake were made. In order to instantly evaluate the 3D displacements and velocities of the GNSS stations at the time of the earthquake in real time, solutions were made with the Kinematic-PPP technique by using the Real-Time satellite orbit and clock information produced by the National Center for Space Studies (CNES) analysis center. In order to verify the results, the final satellite orbit and clock information produced by the German Earth Sciences Research Center (GFZ) were compared together. With the kinematic-PPP solution, 3D position components were obtained in each 24-hour epoch (1 second) of the stations. For the evaluation of the 24-hour solutions obtained, the situation that the earthquake occurred at 01:17:32 according to the UTC time zone and lasted for about 80 seconds was taken as the moment of the earthquake (01:17:32-01:18:52), and the interval of 01:12:32-01:23:52 with 300 seconds before the earthquake and 300 seconds after the earthquake was determined. In order to evaluate the velocity of the GNSS stations at the time of the earthquake, the coordinate differences between two consecutive epochs at the time of the earthquake were obtained. In addition, both horizontal and 3-dimensional vector-based displacement changes were calculated by taking the average coordinate differences of 300 epochs before and after the earthquake of the GNSS stations in the specified time period.

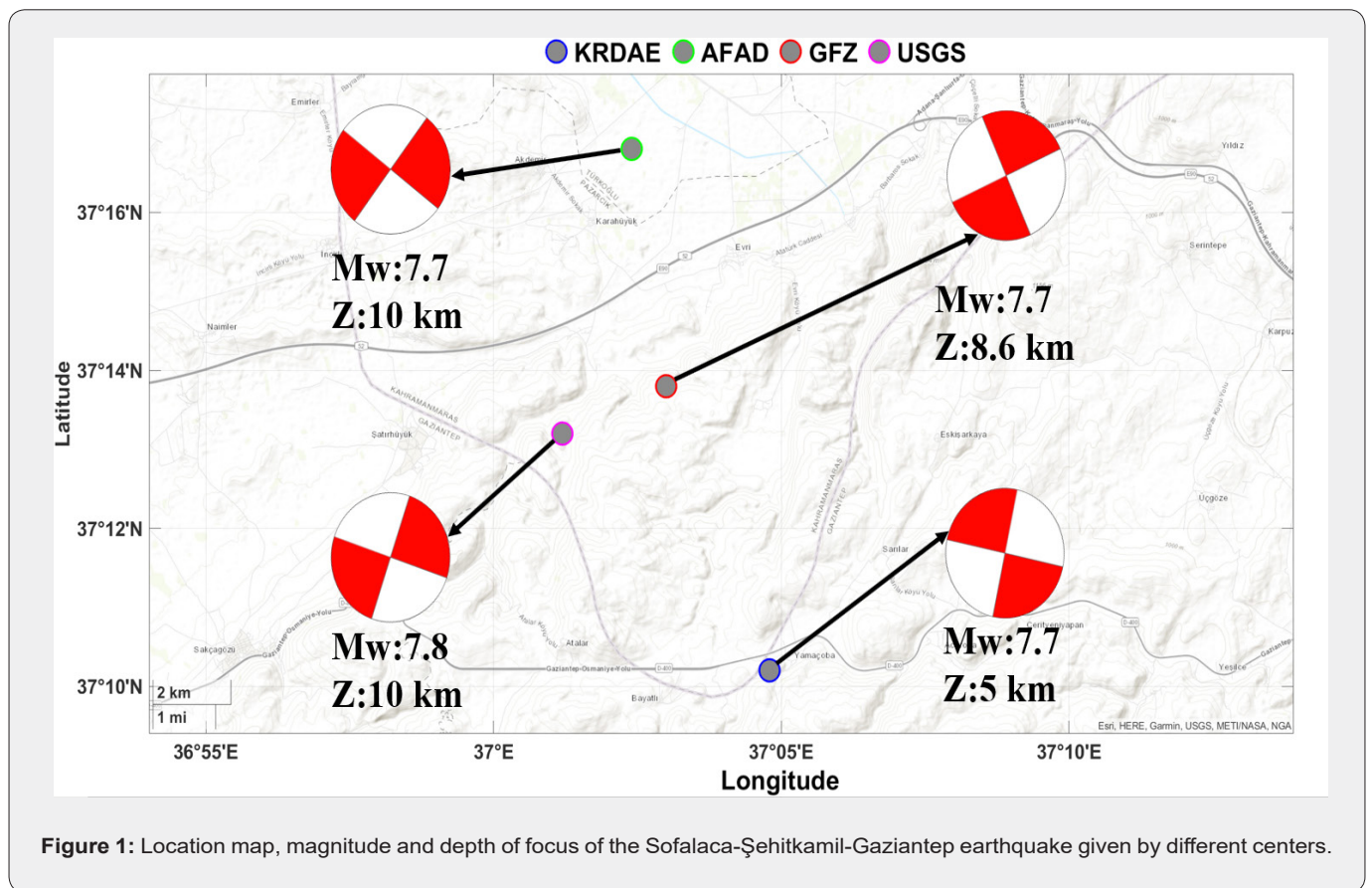


Figure 1: Location map, magnitude and depth of focus of the Sofalaca-Şehitkamil-Gaziantep earthquake given by different centers.



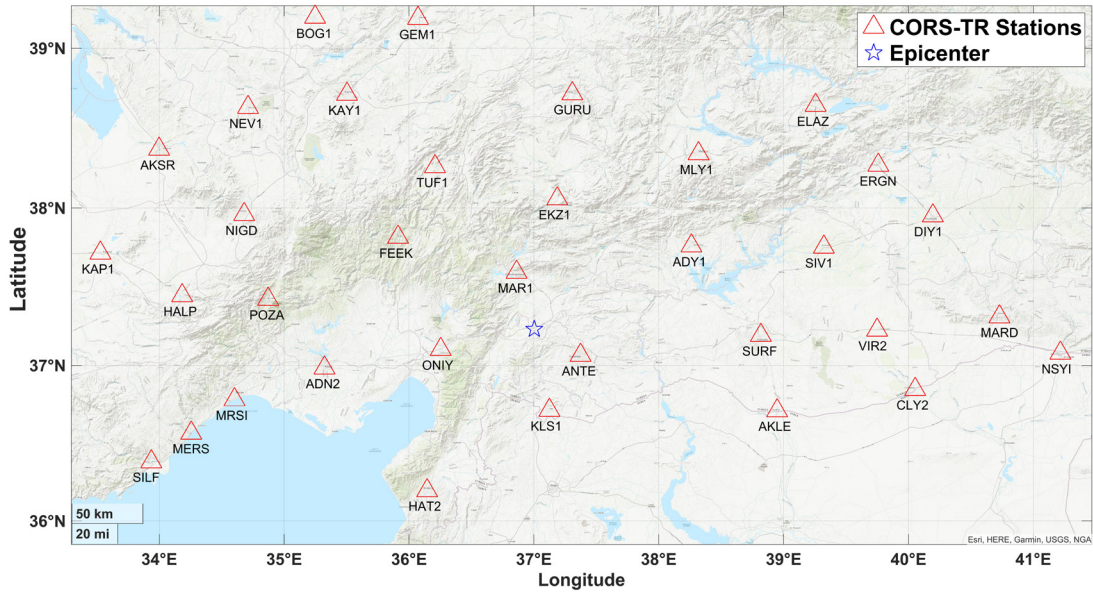


Figure 2: Map of the location of the network of CORS-TR close to the earthquake epicenter.

## Results and Discussion

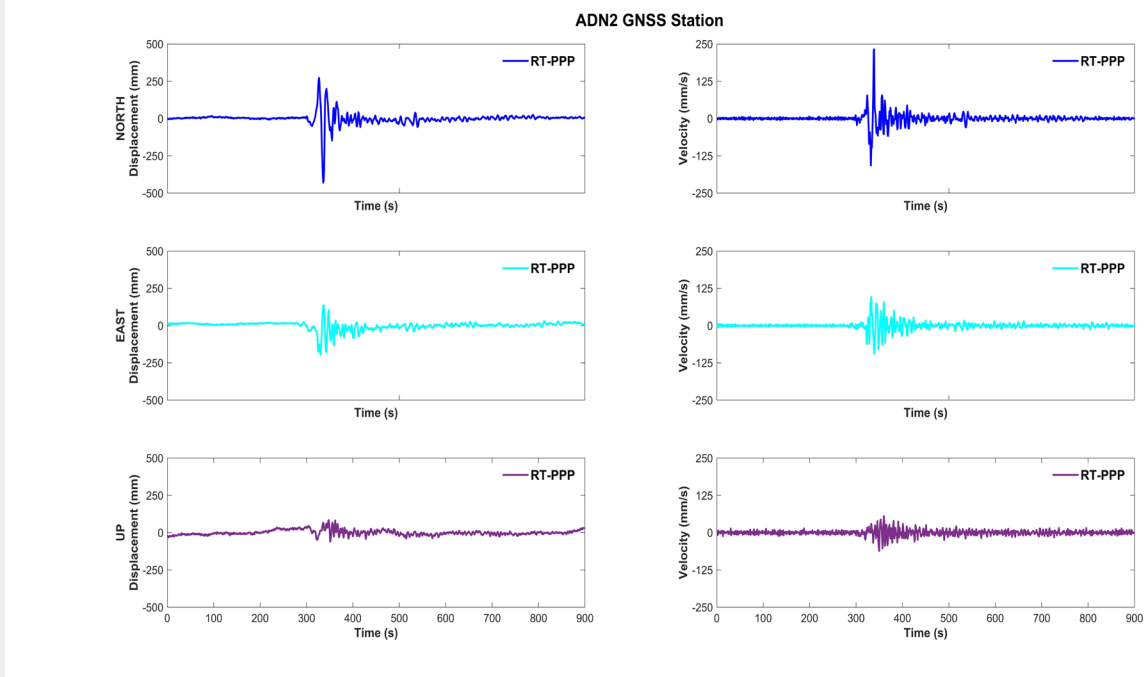


Figure 3: Displacement and velocity time series of the north, east and up components according to the RT-PPP evaluation results for the Sofalaca-Şehitkamil Gaziantep earthquake of the ADN2 GNSS station.

In this section, rapid evaluation of GNSS observations recorded at CORS-TR GNSS stations during the Sofalaca-Şehitkamil earthquake was made under real-time conditions. Surface waveforms, maximum displacements and velocities of all stations were determined. However, only the displacement and velocity time series of ADN2, ANTE and TUF1 stations are shown as examples in the article. The statistical results of the co-seismic displacement amounts, velocities and surface waveforms of all points according to the Final solutions are given in Table 1 & 2 in detail. In Figure 3, the time series of the displacements and velocities of the north, east and up components of the ADN2 station obtained in the RTKLIB software using real-time CNES satellite orbit and clock corrections in the specified time period before, during and after the earthquake are given. A similar situation is illustrated in Figure 4 using Final satellite orbit and clock correction products produced by the GFZ center to test the accuracy of the results.

The maximum velocity values obtained from both real-time and post-process results for the ADN2 station were obtained as 23.3cm/s for the north component, 9.6cm/s for the east component and 6.0cm/s for the up component.

The maximum displacement range occurring in the surface waveform of the ADN2 station at the time of the earthquake is

70.3 [68.6] cm for the north component, 33.0 [32.6] cm for the east component, and 14.3 [14.1] cm for the up component in both solutions. The displacements occurring in the displacement time series show the offset amount of the seismic movements occurring at the time of the earthquake at the location of the GNSS station. However, post-earthquake co-seismic displacements of the ADN2 station are -3.33 [-3.7] cm for the north component, -4.6 [-3.2] cm for the east component, and 1.7 [0.1] cm for the up component. With the calculation of the co-seismic displacements, it was observed that the point of ADN2 was located on the Anatolian Plate relative to the earthquake center as a location, and the horizontal movement of the point took place in the southwest direction. This has led us to interpret that the fault that occurred after the earthquake is left-lateral strike slip. It turns out that there is a heave at this location relative to the displacement in the up component of the ADN2 station.

The displacement and velocity time series of the North, East and Up components of the RT-PPP and PP-PPP solutions of ANTE station, which is one of the stations close to the epicenter of the earthquake, are given in Figure 5 & 6, respectively. In both real-time and post-process solutions of this station, the displacement during the earthquake is 24.5 [24.5] cm for the north component, 37.2 [35.9] cm for the east component, and 14.8 [15.3] cm for the up component.

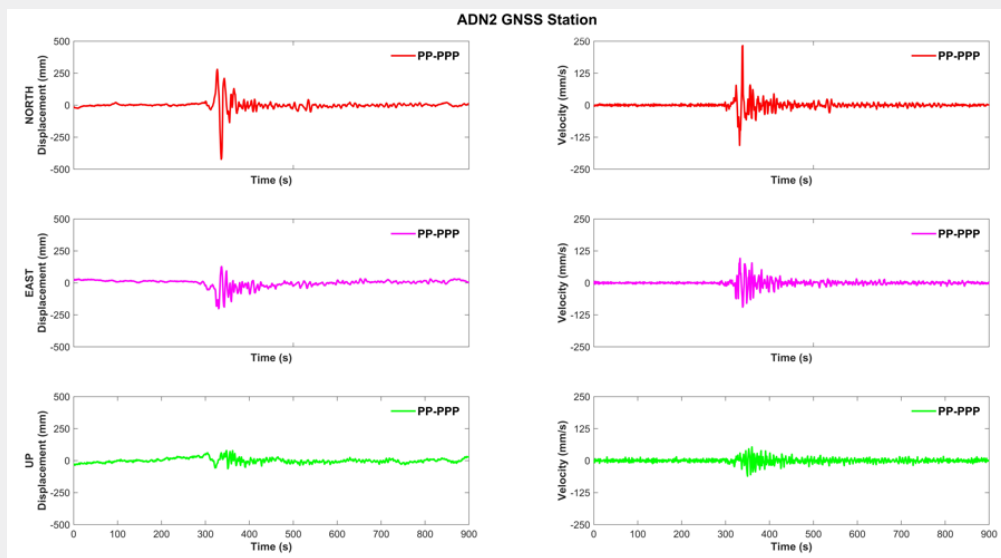


**Figure 4:** Displacement and velocity time series of north, east and up components according to PP-PPP evaluation results for the Sofalaca-Şehitkamil Gaziantep earthquake of ADN2 GNSS station.

In addition, the maximum velocities at the time of the earthquake are 10.3 [10.2] cm/s in the north, 12.0 [11.6] cm/s in the east and 6.1 [5.8] cm/s in the up component. According to the co-seismic displacement results after the earthquake, it is 27.5 [26.5] cm in the north, 22.7 [24.6] cm in the east, and 1.3 [2.2] cm

for the up component. These results show that the ANTE point is located on the Arabian Plate relative to the top of the center and its horizontal movement is towards the northeast. Thus, the interpretation of the movement of the earthquake that occurred on the East Anatolian Fault Zone in the Northeast-Southwest

direction and that it is a left-lateral strike slip was emphasized again. In addition, it is seen that the amount of displacement after the earthquake is greater for the horizontal component than the ADN2 station, depending on the distance from the center of the ANTE station. A post-earthquake heave occurred in the upper component of this station. However, this interpretation can only be made according to the point location. It will be possible to

determine the elevation changes before and after the earthquake by using technologies such as High Resolution Passive (Optical) systems or Active (Radar) systems of the collapses or heaves occurring on the surface of the fault and its vicinity for the analysis on a regional basis. The RT-PPP and PP-PPP results of the MLY1 GNSS station, which we took as the last example and which is close to the epicenter, are given in Figure 7 & 8, respectively.

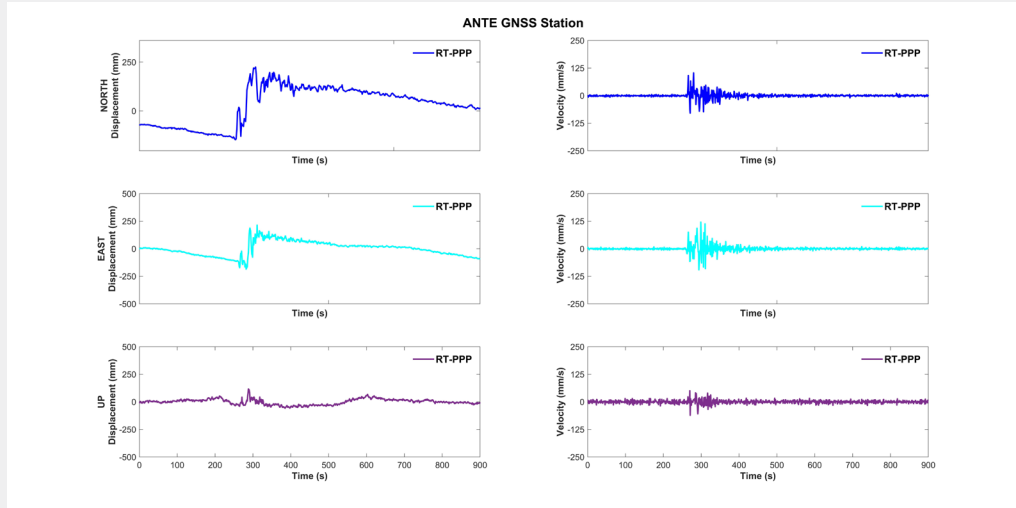


**Figure 5:** Displacement and velocity time series of the north, east and up components according to the RT-PPP evaluation results for the Sofalaca-Şehitkamil Gaziantep earthquake of the ANTE GNSS station.

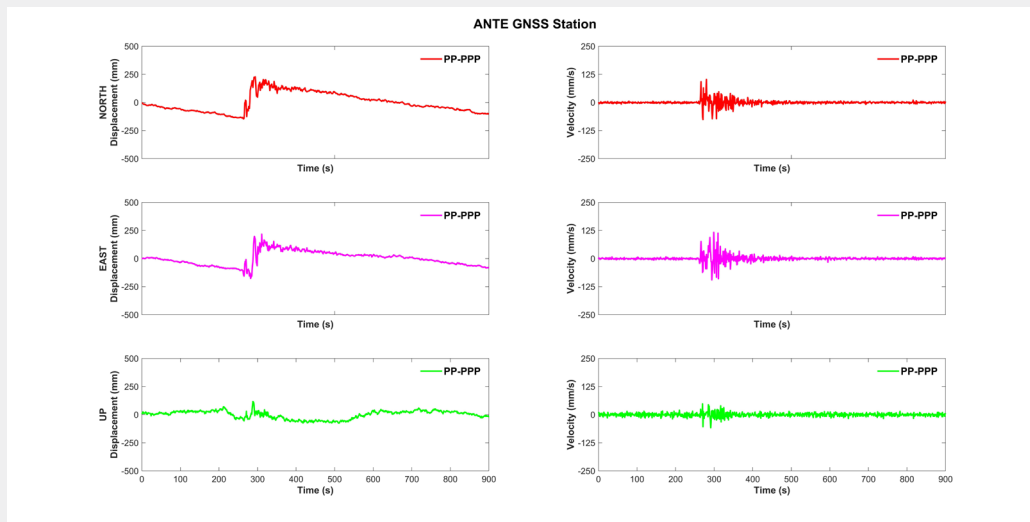


**Figure 6:** Displacement and velocity time series of the north, east and up components according to the PP-PPP evaluation results for the Sofalaca-Şehitkamil Gaziantep earthquake of the ANTE GNSS station.

The maximum surface displacement of the two solution methods at the time of the earthquake is 89.8 [86.9] cm in the north component, 29.9 [29.5] cm in the east component, and 16.2 [16.3] cm in the up component. The maximum displacement at the time of the earthquake is 23.3 [23.3] cm/s, 13.4 [13.3] cm/s and 7.4 [7.6] cm/s for the north, east and up components,

respectively. When all GNSS stations were examined, it was determined that the maximum slip rate and maximum velocity for the north component occurred in this station. In addition, post-earthquake co-seismic displacement results are -37.1 [-37.1] cm, -15.7 [14.4] cm and 3.3 [1.9] cm for the north, east and Up components, respectively. According to the co-seismic results, a

similar interpretation of the ADN2 station can be made here as well. The slip direction is southwest, and maximum co-seismic displacements were observed in the north and Up components relative to all stations. In addition, this is a proof that the GNSS points in the regions close to the center are more affected by the earthquake intensity. It has been observed that the results of the maximum displacement, velocity and co-seismic displacement at the time of the earthquake at the 3 station points taken as an example, in the solutions made using real-time satellite orbit and clock correction information, have similar results compared to the solutions obtained using precise satellite orbit and clock correction products. Horizontal displacements of 34 CORS-TR stations taken

in this study after the Sofalaca-Şehitkamil-Gaziantep earthquake are given in Figure 9. Since 11 stations where GNSS observations were not recorded before and during the earthquake were not included in the solution, the displacements of 23 stations are shown in Figure 9. As can be seen in the figure, the slip rate is higher at locations close to the epicenter of the earthquake, and the amount of strike is smaller at far stations due to the decrease in the intensity of the earthquake with the extension of the distance. In addition, the EAFZ moves in the southwest direction of the stations on the Anatolian plate, while movements in the northeast or east direction have occurred on the Arabian Plate.

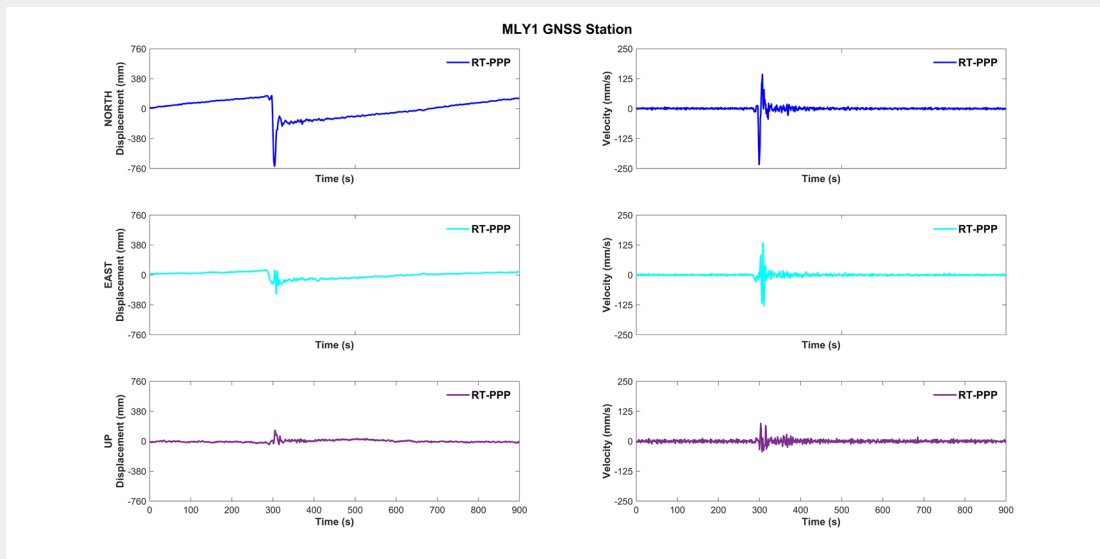


**Figure 7:** Displacement and velocity time series of the north, east and up components according to the RT-PPP evaluation results for the Sofalaca-Şehitkamil Gaziantep earthquake of the MLY1 GNSS station.

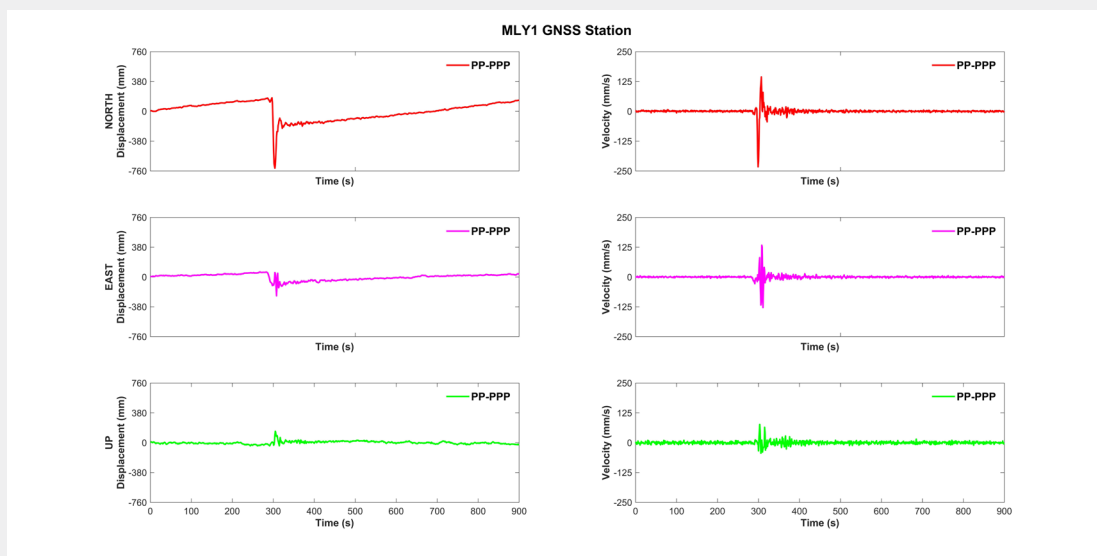


**Figure 8:** Displacement and velocity time series of the north, east and up components according to the PP-PPP evaluation results for the Sofalaca-Şehitkamil Gaziantep earthquake of the MLY1 GNSS station.

The results of the 23 stations shown in Figure 9 are given in Table 1 in detail. The results written in square brackets in Table 1 represent the values obtained from the PP-PPP technique. Looking at the literature, the relative positioning method in Kinematic mode can be used as a comparison criterion for precise evaluation of the results, one rover and the other base. However, in many studies, it has been emphasized that this method limits its use due to the displacement changes that the fixed point is exposed to in large earthquakes. In addition, it is seen once again that the use of the relative positioning method is not appropriate because the intensity of the earthquake that occurred in this study is very large

and its effect is felt in a wide region. However, in many studies in the literature such as GNSS-seismology, Structural Health Monitoring, Early Warning Systems and Rapid Hazard Assessment, it has been proven that PPP-based solutions are made with a single GNSS receiver with cm accuracy after the convergence time of integer phase ambiguity. In this context, in order to test the accuracy of the RT-PPP results of the north, east and Up components of all stations of the maximum displacements and velocities occurring at the time of the earthquake, a comparison was made with reference to the PP-PPP technique. The comparison results are given in Table 2 in detail.

**Table 1:** Maximum displacement, maximum velocity and co-seismic displacements at CORS-TR stations in an earthquake.

ID	NORTH			EAST			UP		
	M. Disp. (cm)	M. Vel. (cm/s)	Co-s. Disp. (cm)	M. Disp. (cm)	M. Vel. (cm/s)	Co-s. Disp. (cm)	M. Disp. (cm)	M. Vel. (cm/s)	Co-s. Disp. (cm)
ADN2	70.3[68.6]	23.3[23.3]	-3.3[-3.7]	33.0[32.6]	9.6[9.6]	-4.6[-3.2]	14.3[14.1]	6.0[6.0]	1.7[0.1]
AKSR	10.7[10.5]	4.8[4.8]	-1.7[-2.0]	9.8[9.5]	5.9[6.3]	-1.6[-0.4]	8.4[8.1]	3.0[2.7]	2.4[1.2]
ANTE	24.5[24.5]	10.3[10.2]	27.5[26.5]	37.2[35.9]	12.0[11.6]	22.7[24.6]	14.8[15.3]	6.1[5.8]	1.3[2.2]
BOG1	21.8[21.6]	4.1[4.1]	-0.6[-0.9]	21.7[21.5]	3.9[3.9]	-2.2[-1.5]	7.1[7.0]	2.4[2.2]	1.7[0.6]
FEEK	13.4[13.2]	4.2[4.3]	-3.2[-3.7]	16.0[14.9]	3.7[3.5]	-6.8[-5.9]	21.6[21.0]	6.0[5.9]	0.3[-0.7]
GEM1	20.8[20.5]	6.5[6.5]	-1.5[-1.7]	39.5[39.9]	9.5[9.7]	-3.2[-1.8]	5.0[5.0]	2.2[2.2]	-1.6[-3.7]
HALP	16.4[16.4]	2.9[2.7]	-0.3[-1.0]	5.5[5.6]	1.7[1.8]	-1.6[-0.4]	7.7[8.5]	2.9[2.9]	-1.7[-3.4]
KAY1	40.6[40.7]	11.5[11.6]	-1.6[-1.7]	28.6[29.2]	6.2[6.3]	-3.7[-2.7]	7.0[7.7]	2.8[3.1]	2.0[0.4]
MLY1	89.8[86.9]	23.3[23.3]	-37.1[-37.1]	29.9[29.5]	13.4[13.3]	-15.7[-14.4]	16.2[16.3]	7.4[7.6]	3.3[1.9]
MRSI	25.3[25.3]	7.5[7.5]	-0.8[-1.1]	13.5[13.3]	4.6[4.4]	-4.3[-2.3]	12.8[13.8]	4.5[4.5]	2.8[-0.3]
NEV1	19.2[19.1]	5.4[5.3]	-0.8[-1.3]	9.0[8.6]	3.6[3.5]	0.1[0.3]	10.8[11.3]	3.3[3.5]	-1.8[-2.2]
POZA	17.5[17.0]	3.8[3.8]	-1.6[-1.6]	6.8[7.2]	1.8[1.8]	-3.3[-2.5]	12.4[11.0]	3.7[3.7]	-2.6[-0.3]
SILF	16.3[15.6]	2.8[2.7]	-0.1[-0.6]	8.5[9.1]	2.1[2.1]	-4.3[-1.6]	9.7[9.0]	2.4[2.2]	1.8[-2.1]
TUF1	33.0[32.7]	9.3[9.2]	-5.8[-6.3]	28.5[28.4]	6.8[6.9]	-3.7[-2.6]	10.4[8.3]	2.5[2.4]	4.7[4.0]
AKLE	32.4[32.0]	12.0[12.2]	-1.2[-2.2]	24.6[24.5]	7.5[7.6]	6.7[7.7]	9.7[10.8]	4.7[4.0]	-1.5[-3.6]
DIY1	1.6[1.4]	1.6[1.1]	2.3[1.9]	1.1[1.0]	0.5[0.4]	-0.1[-0.7]	4.6[3.1]	3.1[1.9]	-3.0[-2.7]
ERGN	63.9[63.7]	18.5[18.4]	0.3[-2.9]	24.4[23.1]	7.2[7.1]	-1.4[6.3]	17.9[17.4]	9.5[8.2]	18.1[18.8]
MERS	18.9[17.3]	3.0[2.9]	-2.1[-2.9]	9.5[9.5]	2.5[2.4]	-1.4[-0.6]	8.8[7.6]	1.9[1.7]	-5.8[-6.2]
NSYI	8.4[9.1]	4.2[3.9]	-1.4[-1.2]	8.3[8.0]	2.8[2.6]	1.8[1.5]	11.8[10.8]	6.2[6.3]	3.8[4.5]
ELAZ	60.3[60.4]	19.2[19.2]	-3.3[-3.6]	33.3[33.1]	6.4[6.4]	-2.1[-1.4]	16.5[15.6]	7.4[7.3]	-0.5[-2.8]
SIV1	36.8[38.1]	14.6[14.5]	-1.5[-1.8]	19.3[19.2]	11.9[12.0]	6.5[7.3]	24.7[25.3]	6.2[7.7]	-2.9[-4.4]
GURU	20.5[20.7]	10.6[10.6]	-8.4[-9.4]	28.7[28.6]	8.5[7.8]	2.3[3.4]	24.6[23.8]	24.6[24.0]	20.0[24.6]
NIGD	6.5[7.1]	3.8[3.9]	-0.7[-1.3]	9.7[9.8]	3.8[3.7]	-2.9[-2.9]	12.2[11.3]	3.6[3.4]	-0.1[-0.5]



**Table 2:** RMSE values of the displacements and velocities of the seismic surface waveform of the earthquake at CORS-TR stations.

Station ID	NORTH		EAST		UP	
	RMSE (mm)	MAX (mm)	RMSE (mm)	MAX (mm)	RMSE (mm)	MAX (mm)
ADN2	7	19.4	6.7	14.5	6.9	18.2
ADN2 (Velocity)	0.7	1.9	0.6	2	1	3.4
AKSR	4.4	11.6	4.8	10.4	7.3	19.6
AKSR (Velocity)	1	3.1	1	3.4	1.7	4.9
ANTE	5.7	14.6	6.1	16.5	19.8	41.3
ANTE (Velocity)	1.3	3.6	1.3	4.1	2.1	11.4
BOG1	3.9	10.2	4.8	11.1	7	19.5
BOG1 (Velocity)	1	3.1	1	4	1.7	4.4
FEEK	4.9	17.2	5.2	11.9	11.2	30
FEEK (Velocity)	1.2	4.3	1.2	3.8	2	6.3
GEM1	4.6	11.3	4.6	11.3	7.5	22.1
GEM1 (Velocity)	1	2.9	1.1	3.5	1.8	5.4
HALP	4.4	11.6	5	12.2	7.3	20.7
HALP (Velocity)	1.1	3.8	1.1	3.3	1.8	5.9
KAY1	4.5	11.2	4.9	12.4	7.4	20.4
KAY1 (Velocity)	1	3	1.1	3.7	1.7	5.1
MLY1	4.6	10.6	4.7	13.3	7.1	22.1
MLY1 (Velocity)	1.1	3.8	1.1	3.7	1.7	4.9
MRSI	4.1	9	6.2	13.5	7.7	21.9
MRSI (Velocity)	1	3.5	1	4.1	1.7	4.9
NEV1	4.1	10.7	7.8	15.9	8.7	25.7
NEV1 (Velocity)	1	2.9	1	3	1.7	5.4
POZA	4.1	9.8	7.3	20.7	12.9	29.9
POZA (Velocity)	1.2	4.2	1	3.5	1.8	5.5
SILF	4	9.3	4.9	10.5	7.5	20.1
SILF (Velocity)	1	3.2	1	3.5	1.8	5
TUF1	7.1	19.5	6.9	14.3	7	19.6
TUF1 (Velocity)	0.7	2.1	0.5	1.8	1	3.1
AKLE	5.2	13.2	8.4	20.1	8.9	29.1
AKLE (Velocity)	1.6	2.3	1.6	8.6	2.3	9
DIY1	4.7	14.4	4.8	11.3	7.9	25
DIY1 (Velocity)	0.9	4.4	0.6	1.8	3	10.4
ERGN	7.7	18.2	24.1	44	25.3	81.3
ERGN (Velocity)	2.6	13.5	4	18.7	9.4	54.7
MERS	4.9	10.3	4.5	10.2	7.1	18.3
MERS (Velocity)	0.9	2.3	0.9	3.3	1.5	3.9
NSYI	6.1	21.3	7.1	16.8	14.9	38
NSYI (Velocity)	1.9	6.3	2.7	9	5.1	15.5
ELAZ	3.9	9.1	5.4	12.8	6.7	20.5
ELAZ (Velocity)	1	2.8	1.1	3.4	1.6	4.8
GURU	4.9	12.5	5.3	14.5	11.8	34.4
GURU (Velocity)	1.2	3	1.2	6.5	1.9	7.6
SIV1	4.1	10.3	4.3	12.4	6.9	23

SIV1 (Velocity)	1.1	4.1	1.1	4.4	1.6	5
NIGD	4.3	10	4.4	13.1	7.1	19.8
NIGD (Velocity)	1	3.3	1	3.6	1.7	5.4

According to Table 2, successful results were obtained under cm for the horizontal component and approximately 1cm for the up component. Thus, instant evaluations can be made to monitor, detect and analyze dynamic surface movements that occur during an earthquake. This is important to evaluate the characteristics of the Earth's crust and engineering structures (High-Rise Building, Hospital, Shopping Center, Bridge, Stadium, Viaduct, Tower, etc.) to dynamic movements that occur during an earthquake in real time. In Table 1, the maximum displacement, maximum velocity and co-seismic displacements at the time of the earthquake are

given in then north, east and up components. The values in this table are shown in Figure 10-12 for the maximum displacement, maximum velocity, and co-seismic displacements for the north, east, and up components, respectively. Maximum displacement, maximum velocity and co-seismic displacements occurring in the northern component of CORS-TR stations show slight differences at the millimeter level for both real-time solutions and post-process solutions. A similar situation is given for the eastern component as seen in Figure 11.

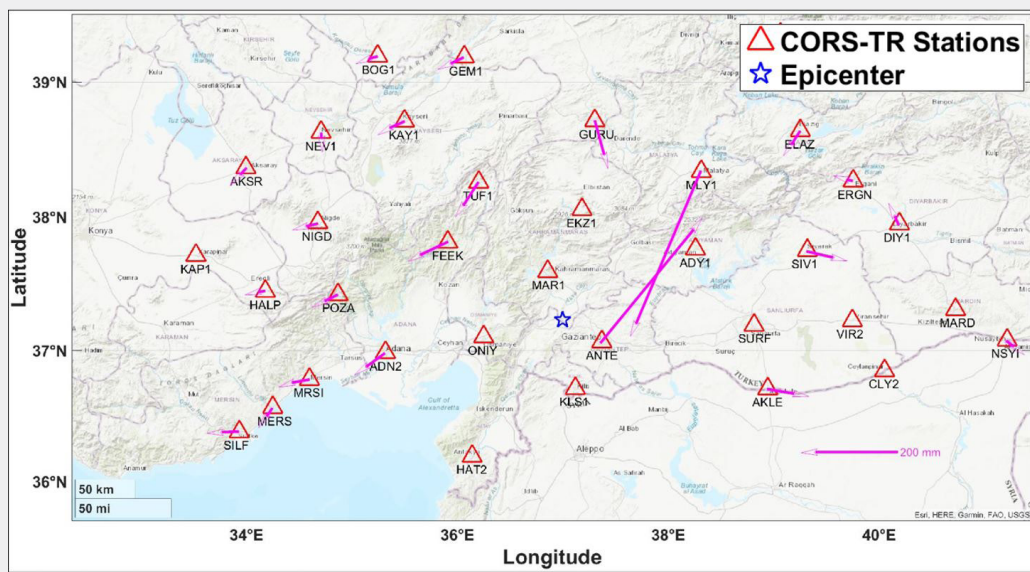


Figure 9: Horizontal slip rates caused by the Sofalaca-Şehitkamil Gaziantep (Mw:7.7) earthquake.

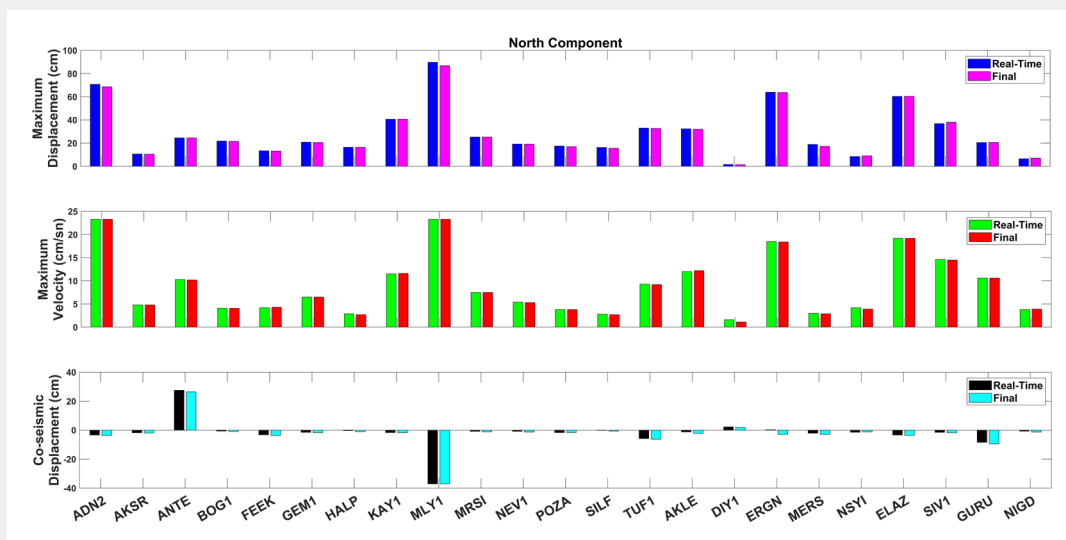
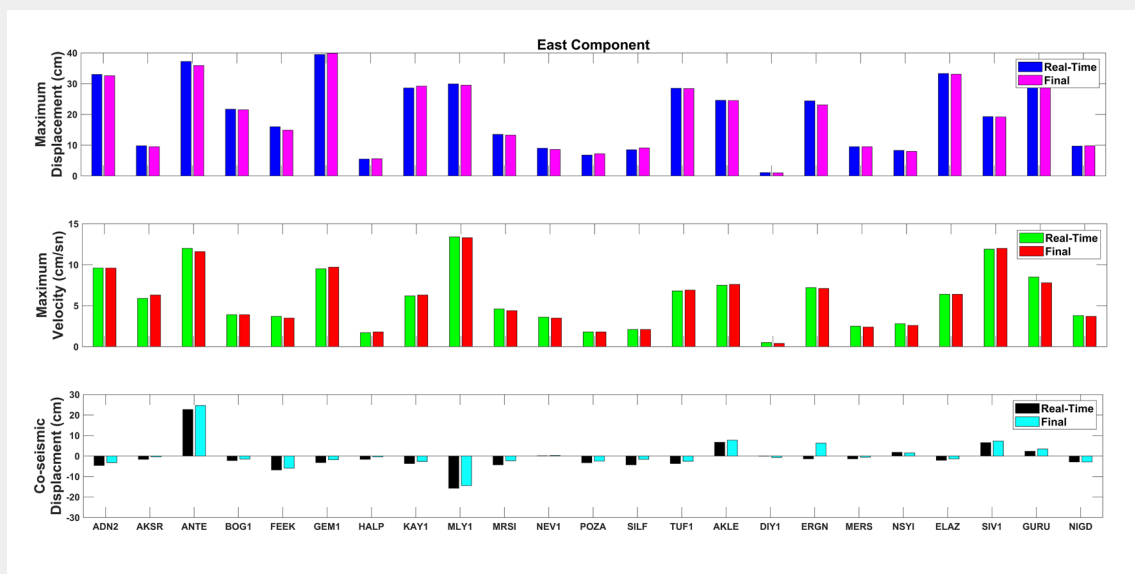
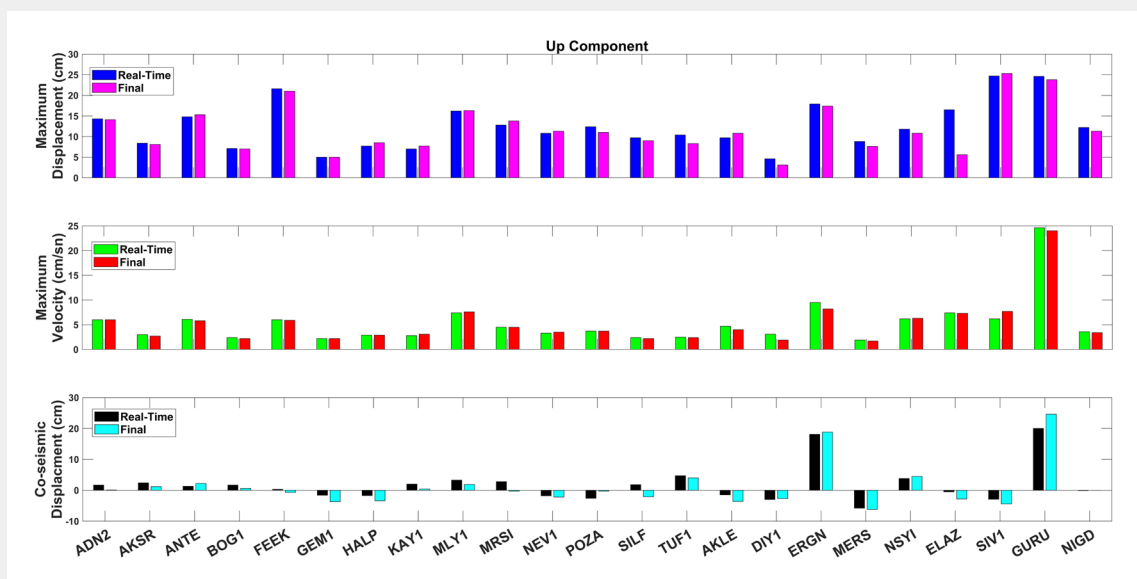


Figure 10: Maximum displacement, maximum velocity and co-seismic displacements caused by the north component of CORS-TR stations of the Sofalaca-Şehitkamil Gaziantep (Mw:7.7) earthquake.



**Figure 11:** Maximum displacement, maximum velocity and co-seismic displacements caused by the east component of CORS-TR stations of the Sofalaca-Şehitkamil Gaziantep (Mw:7.7) earthquake.



**Figure 12:** Maximum displacement, maximum velocity and co-seismic displacements caused by the up component of CORS-TR stations of the Sofalaca-Şehitkamil Gaziantep (Mw:7.7) earthquake.

Although the maximum displacement and maximum velocities in the eastern component of CORS-TR stations are slightly different in millimeters for both real-time solutions and post-process solutions, there are centimeter-level differences in co-seismic displacements at some stations. A similar situation for the up component is given in Figure 12.

As can be seen in Figure 12, the results of the maximum displacement and velocity values of the up component are

consistent with each other at the millimeter level in both real-time and post-process solutions. However, there were centimeter-level differences in the co-seismic displacements of the upper component at some stations.

In Table 2, the RMSE values of the displacements and velocities at the time of the earthquake of 23 CORS-TR stations are given. The RMSE values of the displacement and velocity components of the north, east and up components of the stations

are shown in Figure 13. It is clear from the figure that the northern component of the stations is more accurate than the other components. Considering the GNSS observations, it can be interpreted that the GPS and GLONASS satellite constellations are

determined with different sensitivity in their orbital direction and components perpendicular to the orbital direction, and that the satellite systems are in the north-west direction, and the northern components of the stations give more precise results.

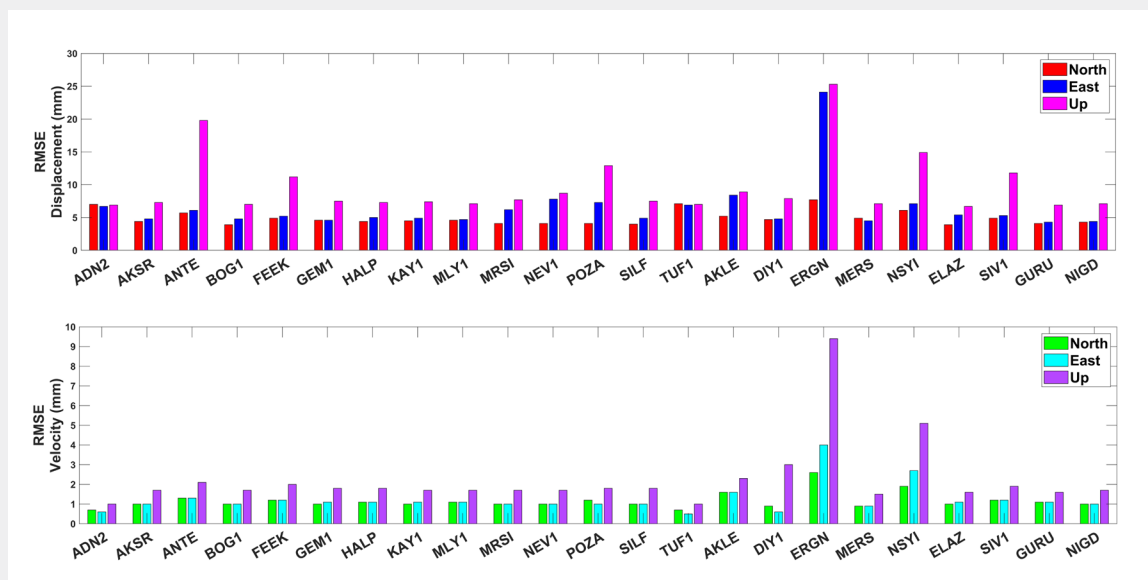


Figure 13: RMSE values of the displacement and velocity of the Sofalaca-Şehitkamil Gaziantep (Mw:7.7) earthquake at CORS-TR stations.

**Conclusion**

In this study, seismic surface movements, maximum displacements and velocities, co-seismic displacements, which occurred after the Sofalaca-Şehitkamil Gaziantep earthquake, were geodesically evaluated in RTKLIB software by taking 34 of GNSS station data sets homogeneously distributed over the earthquake center from CORS-TR GNSS stations. The Kinematic-PPP results performed with the RTKLIB software were calculated as 23.3cm/secs at the MLY1 station with the highest speed in the north component at the time of the earthquake, about 13.4cm/s at the MLY1 station with the highest speed in the east component, and approximately 7.4cm/s at the ELAZ and MLY1 stations in the up component. According to the results of the post-earthquake co-seismic displacement, it is -37.1cm at the MLY1 station at the most in the northern component, 22.68cm at the ANTE station in the eastern component, and 4.7cm at the highest TUF1 station in the up component. According to the post-earthquake geodetic results, it was observed that most of the CORS-TR GNSS station points in the western block of the fault surface, namely the Anatolian plate, were displaced in the southwest direction on a vector basis in the horizontal component. A similar situation is that most of the GNSS stations remaining in the eastern block of the fault surface, namely the Arabian Plate, have been displaced in the north or northeast direction. This situation made the interpretation that the earthquake generally has left-slip strike fault type at the

surface. In addition, when looking at the locations of the stations, it can be said that there are heaves at some points and collapses at others. Most of the GNSS station data sets taken while evaluating the GNSS data sets include GPS and GLONASS observations. In many studies in the literature, it has been observed that the position accuracy increases in processes made with Multi-GNSS observations. However, it is clear that the renewal of 168 GNSS stations in the CORS-TR system located in Türkiye and the [Turkish Republic of Northern Cyprus \(TRNC\)](#) with a GNSS receiver/antenna that makes observations on GPS, GLONASS, BeiDou and Galileo satellite systems on a global scale will be evaluated with more geodetic accuracy in regional earthquakes. In Türkiye, an average of 10 to 20 satellite observations can be made from BeiDou and Galileo satellite systems. Galileo satellite systems should be included for all GNSS stations in order for the GPS, GLONASS and BeiDou satellite systems to be for military purposes in the global sense and to prevent the CORS-TR system from being affected due to the problems arising from international strategic conflicts in the future. In addition to the technological developments that Türkiye has made in many fields, the development of a regional satellite system with the partnership of the Turkish Space Research Institute and related institutions and its integration into the CORS-TR System will create a new trend in many application areas in the geodetic sense.



## Acknowledgment

We thank the General Directorate of Land Registry and Cadastre (TKGM) and the General Directorate of Maps (HGM) for the network of CORS-TR data used in this study. We also thank Researcher Tomoji Takasu for the open source RTKLIB software used for RT-PPP and PP-PPP solution approaches in this study, and the National Center for Space Studies (CNES) and the German Geosciences Research Center (GFZ) for providing Multi-GNSS satellite orbit and clock correction products.

## References

- D Mckenzie (1970) Plate Tectonics of the Mediterranean Region. *Nature* 226(5242): 239-243.
- D Mckenzie (1972) Active tectonics of the mediterranean region. *Geophysical Journal International* 30(2): 109-186.
- E Bozkurt, SK Mittweide (2001) Introduction to the geology of Türkiye—a synthesis. *International Geology Review* 43(7): 578-594.
- R Reilinger, S McClusky, P Vernant, S Lawrence S Ergintav, et al. (2006) GPS constraints on continental deformation in the Africa-Arabia-Eurasia continental collision zone and implications for the dynamics of plate interactions. *Journal of Geophysical Research* 111: B05411.
- H Yavasoglu, E Tari, B Tüysüz, Z Çakır, S Ergintav (2011) Determining and modeling tectonic Movements along the central part of the North Anatolian fault (Türkiye) using geodetic measurements. *Journal of Geodynamics* 51(5): 339-343.
- AMC Şengör (1979) The North Anatolian transform fault: its age, offset and tectonic significance. *Journal of the Geological Society of London* 136(3): 269-282.
- Ö Emre, TY Duman, S Özalp, H Elmacı, Ş Olgun, et al. (2013) Active fault map of Türkiye with an explanatory text 1:1,250,000 scale. General Directorate of Mineral Research and Exploration Special Publication Series 30.
- E Arpat, F Şaroğlu (1972) The East Anatolian Fault System; Thoughts on its Development. *Journal of Mineral Research and Exploration Institute of Türkiye* 78: 33-39.
- F Şaroğlu, Ö Emre, I Kuşçu (1992) The East Anatolian Fault zone of Türkiye. *Annals Tectonics* 6: 99-125.
- MA Özdemir, M İnceöz (2003) Comparison of the Offsets in Drainage Network with Some Tectonic Data between Karlıova-Türkoğlu in the East Anatolian Fault Zone. *Afyon Kocatepe University Journal of Social Sciences* 5(1): 89-114.
- O Emre, TY Duman, F Ozalp, F Saroglu, S Olgun (2018) Active fault database of Türkiye. *Bulletin of Earthquake Engineering* 16(8): 3229-3275.
- SS Yıldız, A Ozkan, HH Yavasoglu, F Masson, I Tiryakioglu, et al. (2020) Determination of recent tectonic deformations in the vicinity of Adana-Osmaniye-Hatay-Gaziantep triple junction region by half-space modeling. *Comptes Rendus. Géoscience* 352(3): 225-234.
- B Aktug, H Ozener, A Dogru, A Sabuncu, B Turgut, et al. (2016) Slip rates and seismic potential on the East Anatolian Fault System using an improved GPS velocity field. *Journal of Geodynamics* 94-95: 1-12.
- J Kouba (2003) Measuring Seismic Waves Induced by Large Earthquakes with GPS. *Studia Geophysica et Geodaetica* 47: 741-755.
- P Xu, C Shi, R Fang, J Liu, X Niu, et al. (2013) High-rate precise point positioning (PPP) to measure seismic wave motions: an experimental comparison of GPS PPP with inertial measurement units. *Journal of Geodesy* 87(4): 361-372.
- Z Nie, R Zhang, G Liu, Z Jia, D Wang, et al. (2016) GNSS seismometer: Seismic phase recognition of real-time high-rate GNSS deformation waves. *Journal of Applied Geophysics* 135: 328-337.
- I Tiryakioglu, CO Yigit, H Yavasoglu, MH Saka, RM Alkan (2017) The Determination of interseismic, coseismic and postseismic deformations caused by the Gökçeada-Samothraki earthquake (2014, Mw: 6.9) based on GNSS Data. *Journal of African Earth Sciences* 133: 86-94.
- J Paziewski, R Sieradzki, R Baryla (2018) Multi-GNSS high-rate RTK, PPP and novel direct phase observation processing method: Application to precise dynamic displacement detection. *Measurement Science and Technology* 29(3): 035002.
- CO Yigit, M Bezcioglu, V Ilci, IM Ozulu, RM Alkan, et al. (2022) Assessment of Real-Time PPP with Trimble RTX correction service for real-time dynamic displacement monitoring based on high-rate GNSS observations. *Measurement* 201: 111704.
- M Bezcioglu, CO Yigit, B Karadeniz, AA Dindar, A El-Mowafy, et al. (2023) Evaluation of real-time variometric approach and real-time precise point positioning in monitoring dynamic displacement based on high-rate (20 Hz) GPS Observations. *GPS Solutions* 27(1): 43.
- A Avallone, M Marzario, A Cirella, A Piatanesi, A Rovelli, et al. (2011) Very high rate (10 Hz) GPS seismology for moderate-magnitude earthquakes: the case of the Mw6.3 LAquila. (central Italy) event. *Journal of Geophysical Research* 116: B02305.
- F Moschas, SC Stiros (2014) Three-dimensional dynamic deflections and natural frequencies of a stiff footbridge based on measurements of collocated sensors. *Structural Control and Health Monitoring* 21(1): 23-42.
- N Takahashi, Y Ishihara, H Ochi, T Fukuda, J Tahara, et al. (2014) New buoy Observation system for tsunami and crustal deformation. *Marine Geophysical Research* 35(3): 243-253.
- CO Yigit (2016) Experimental assessment of post-processed kinematic precise point positioning method for structural health monitoring. *Geomatics, Natural Hazards and Risk* 7(1): 363-380.
- CO Yigit, G Eralp (2017) Experimental testing of high-rate GNSS precise point positioning (PPP) method for detecting dynamic vertical displacement response of engineering structures. *Geomatics, Natural Hazards and Risk* 8(2): 893-904.
- X Tang, GW Roberts, X Li, C Hancock (2017) Real-time kinematic PPP GPS for structure monitoring applied on the Severn suspension bridge, UK. *Advances in Space Research* 60(5): 925-937.
- MR Kaloop, CO Yigit, JH Hu (2018) Analysis of the dynamic behavior of structures using the high-rate GNSS-PPP method combined with a wavelet-neural model: Numerical simulation and experimental tests. *Advances in Space Research* 61(6): 1512-1524.
- MR Kaloop, CO Yigit, AA Dindar, M Elshawary, JW Hu (2020) Evaluation of the high-rate GNSS-PPP method for vertical structural motion. *Survey Review* 52(371): 159-171.
- MR Kaloop, CO Yigit, A El-Mowafy, M Bezcioglu, AA Dindar, et al. (2020) Evaluation of multi-GNSS high-rate relative positioning for monitoring dynamic structural movements in the urban environment. *Geomatics Natural Hazards and Risk* 11(1): 2239-2262.
- CO Yigit, A El-Mowafy, AA Dindar, M Bezcioglu, I Tiryakioglu (2021) Investigating Performance of High-Rate GNSS-PPP and PPP-AR for Structural Health Monitoring: Dynamic Tests on Shake Table. *Journal of Surveying Engineering* 147(1): 05020011.
- S McClusky, S Balassanian, A Barka, C Demir, S Ergintav, et al. (2000) Global positioning system constraints on plate kinematics and dynamics in the eastern Mediterranean and Caucasus. *Journal of Geophysical Research Atmospheres* 105(B3): 5695-5719.

32. E Herece (2003) East Anatolian Fault. Earthquake and Urbanization, Türkiye.
33. R Westaway (2003) Kinematics of the Middle East and Eastern Mediterranean Updated. Turkish Journal of Earth Sciences 12(1): 5-46.
34. H Özener, E Arpat, S Ergintav, A Doğru, R Çakmak, et al. (2010) Kinematics of the eastern part of the North Anatolian Fault Zone. Journal of Geodynamics 49(3-4): 141-150.
35. O Cavalié, S Jónsson (2014) Block-like plate movements in eastern Anatolia observed by InSAR. Geophysical Research Letters 41(1): 26-31.
36. RJ Walters, B Parsons, TJ Wright (2014) Constraining crustal velocity fields with InSAR for Eastern Türkiye: limits to the block-like behavior of Eastern Anatolia. Journal of Geophysical Research 119(6): 5215-5234.
37. R Demirtaş (2003) DAFZ'nda Deprem Üreten Diri Faylar; 1900-2003 Yılları Arasında Doğu Anadolu Fay Zonunda Olmuş Hasar Yapıcı Depremler. Earthquake and Urbanization, Türkiye.
38. O Tatar, H Sözbilir, E. Bozkurt, E Aksoy, F Koçbulut, et al. (2020) 24 Ocak 2020 Sivrice (Elazığ)-Doğanyol (Malatya) Depremi: Arazi Gözlemleri ve Değerlendirilmesi. TMMOB Chamber of Geological Engineers 145.
39. Boğaziçi University Kandilli Observatory and Earthquake Research Institute-Regional Earthquake Tsunami Monitoring and Evaluation Center (2023) 06 February 2023 Sofalaca-Sehitkamil-Gaziantep; Ekinözü-Kahramanmaraş and February 20, 2023 Hatay Earthquakes Preliminary Evaluation Report.
40. T.C. Ministry of Interior Disaster and Emergency Management Presidency (2023) 06 February 2023 Kahramanmaraş (Pazarcık and Elbistan) Earthquakes Field Studies Preliminary Evaluation Report.



This work is licensed under Creative Commons Attribution 4.0 License  
DOI: [10.19080/IJESNR.2023.32.556335](https://doi.org/10.19080/IJESNR.2023.32.556335)

**Your next submission with Juniper Publishers  
will reach you the below assets**

- Quality Editorial service
- Swift Peer Review
- Reprints availability
- E-prints Service
- Manuscript Podcast for convenient understanding
- Global attainment for your research
- Manuscript accessibility in different formats  
**( Pdf, E-pub, Full Text, Audio )**
- Unceasing customer service

**Track the below URL for one-step submission**  
<https://juniperpublishers.com/online-submission.php>